



# A model for the depth-dependence of receptive field size and contrast sensitivity of cells in layer 4C of macaque striate cortex

Ute Bauer <sup>a,\*</sup>, Michael Scholz <sup>c</sup>, Jonathan B. Levitt <sup>b</sup>, Klaus Obermayer <sup>c</sup>,  
Jennifer S. Lund <sup>b</sup>

<sup>a</sup> Technische Fakultät, AG Neuroinformatik, Universität Bielefeld, PO-Box 10 01 31, D-33501 Bielefeld, Germany

<sup>b</sup> Department of Visual Science, Institute of Ophthalmology, Bath Street, London EC1 V 9EL, UK

<sup>c</sup> FB Informatik, FR 2-1, Technische Universität Berlin, Franklinstraße 28-29, D-10587 Berlin, Germany

Received 17 September 1997; accepted 9 March 1998

---

## Abstract

A model of LGN-input to layer 4C of macaque primary visual cortex has been used to test the hypothesis that feedforward convergence of P- and M-inputs onto layer 4C spiny stellate neurons is sufficient to explain the observed gradual change in receptive field size and contrast sensitivity with depth in the layer. Overlap of dendrites of postsynaptic neurons between M- and P-input zones proved sufficient to explain change in the lower two-thirds of layer 4C, while more rapid change in upper 4C was matched by proposing two different M-inputs with partial overlap in upper 4Cz. © 1998 Elsevier Science Ltd. All rights reserved.

*Keywords:* Receptive field; Contrast; Area V1; M and P channels; Computational

---

## 1. Introduction

The aim of our modeling work is to develop sound hypotheses about cortical circuits of macaque monkey primary visual cortex where details of the actual circuitry are difficult to explore experimentally. We wish to determine how the neuron response properties of layer 4C (the primary input zone of thalamic fibers) are generated—specifically, to what degree the response properties of the thalamic recipient spiny stellate neurons of layer 4C can be explained simply on the basis of convergent feedforward excitation from the lateral geniculate nucleus (LGN). There has been a great deal of interest in exploring how cortical orientation and direction selectivity could arise from direct thalamic fiber convergence (reviewed by Das, 1996), but the emergence of more basic response properties, like receptive field size and achromatic contrast sensitivity—on which other response properties depend—has been surprisingly little investigated. The present study is a first attempt to fill this gap. The knowledge about the generation of basic response properties can then be

used as a sound base to address for the first time realistic neural circuitry for generating other response properties of cortical neurons.

Layer 4C is of particular importance since it is the principal recipient zone of two major channels of information, provided by the M and P ganglion cells of the retina (Leventhal, Rodieck & Dreher, 1981). These channels relay through the magnocellular (M) and parvocellular (P) layers respectively of the LGN to cortical area V1; the M fibers terminate in the upper,  $\alpha$ , division of 4C and the P fibers terminate in the lower,  $\beta$ , half of the layer (Hubel & Wiesel, 1972; Blasdel & Lund, 1983). Three separate relays, with cells of origin staggered in depth of the layer, pass from layer 4C to different strata in the more superficial cortex, each stratum containing key sets of efferent neurons (Yoshioka, Levitt & Lund, 1994). The model attempts to establish how the thalamic afferents distribute on postsynaptic excitatory neurons of layer 4C to produce the pattern of physiological response properties recorded in depth of the layer.

We interpret the responses of the neurons of layer 4C from top to bottom of the layer, as observed in the studies of Blasdel & Fitzpatrick (1984) and Hawken & Parker (1984), as a gradient in achromatic contrast

---

\* Corresponding author. Tel.: +49 30 31473442; fax: +49 30 31473121; e-mail: oby@cs.tu-berlin.de.

sensitivity and receptive field size between the afferent M and P properties. It is this functional gradient that we are seeking to replicate in our model, and how it emerges from the initial entry of thalamic information in two non overlapping territories. The model is based on purely monocular ON input from the LGN and considers first two thalamic input channels, M and P, with biologically appropriate anatomical and physiological properties. Secondly, the model considers three thalamic channels, where the M pathway contains two fiber components, M1 and M2, terminating in two partially overlapped zones, M1, occupying the upper half of layer  $4C\alpha$  and M2, occupying the full depth of the  $\alpha$  division. Examples of these two M populations are found in the anatomical studies of Blasdel & Lund (1983) and Freund, Martin, Soltesz, Somogyi & Whitteridge (1989).

The results of our modeling work using purely feed-forward simulated thalamic input persuade us that dendritic overlap by spiny stellate neurons in depth of 4C, especially across the boundary between  $\alpha$  and  $\beta$  divisions, is an important factor leading to the observed physiological gradient between M and P properties in depth of the layer. However this overlap is not sufficient to account for the precise shape of the gradient in contrast sensitivity and receptive field size recorded in neurons through the depth of layer 4C. Only when we include two partially overlapped populations of M-fiber-inputs, each emphasising somewhat different functional properties within the range of values recorded in the LGN, do we achieve a near perfect match to the real contrast sensitivities and field sizes seen in depth of the layer.

The physiological properties of LGN neurons in M and P layers, accurate arbor size and degree of overlap of thalamic axon arbors and appropriate vertical spread of spiny stellate neuron dendritic arbors are fundamental to our model. Therefore, the first part of the paper reviews the relevant anatomical and physiological properties used to constrain the model. The detailed network architecture, the mathematical description of the model neuron and the algorithms which were used to establish realistic connectivity and reasonable transfer functions for our model neurons follow this review. Although sophisticated mathematical theories exist that allow detailed modeling of morphological and biophysical features of single neurons, we believe this level of detail unnecessary to test the nature of projections to layer 4C. The most compelling reasons, however, to discard a more sophisticated compartmental model approach are the lack of precise experimental values for the biophysical parameters of the neurons involved and the large numbers of cells that must be modelled in order to obtain quantitative predictions. The third part of the paper presents the numerical results of our modelling study; this is followed by a discussion of the

likelihood of this circuitry versus other possibilities and suggestions for new experiments that may confirm or refute the circuitry suggested by the model. Preliminary accounts of our exploratory models have been presented previously (Lund, Levitt & Wu, 1994; Wu, Lund & Levitt, 1994; Lund, Wu, Hadingham & Levitt, 1995; Bauer, Scholz, Levitt, Obermayer & Lund, 1997).

## 2. Anatomical and physiological background

### 2.1. Overview of relevant anatomical findings

Fig. 1 summarises our anatomical observations of layer 4C (see Lund, 1990). Studies of the terminal fields of single thalamic axons (Blasdel & Lund, 1983) show that the axon terminals of single LGN-P cells are restricted to  $4C\beta$  (i.e. half the depth of layer 4C—see Blasdel & Lund (1983), for laminar boundary positions, which are best defined by cytochrome oxidase–CO–staining); each P axon terminal field has an approximately circular axon spreading in the lateral dimension

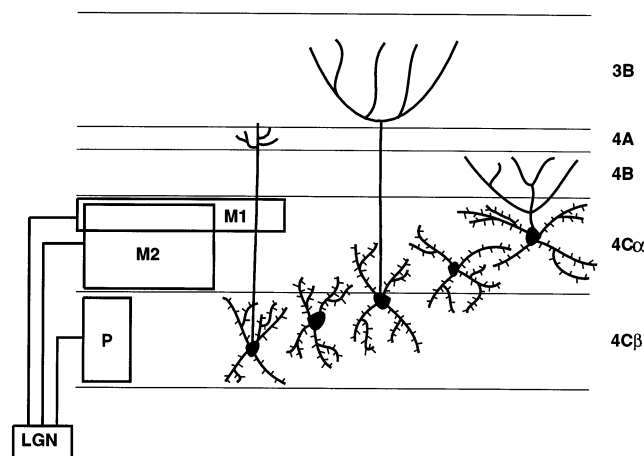


Fig. 1. Anatomical organization of LGN-inputs into layer 4C of macaque monkey primary visual cortex, together with the dendritic organisation and axon projections of the postsynaptic spiny stellate neurons within the layer (modified from Lund, 1990). The LGN afferents entering layer 4C in V1 can be divided into three sets: P fibers from the parvocellular LGN layers, and two sub-groups of fibers, M1 and M2, from the LGN-M layers: P axons terminate only in layer  $4C\beta$ , M2 axons cover the whole depth of layer  $4C\alpha$ , and M1 axons occupy only the top half of layer  $4C\alpha$ . Note that the existence of two M fiber groups is supported by both anatomical studies which have examined M axon morphologies by intracellular filling techniques: Blasdel & Lund (1983), Freund, Martin, Soltesz, Somogyi & Whitteridge (1989) and personal communication; Lund (1990). See text for further discussion. Within layer 4C, spiny stellate neurons are the major postsynaptic targets of LGN axon terminals. Through the depth of layer 4C, these spiny stellate cells have dendritic overlap over one another. Particularly, cells in the mid layer 4C have dendritic intrusion into both  $4C\alpha$  and  $4C\beta$  regions. Outputs from the layer form three sets from top to bottom of the layer: to layer 4B from cells in upper 4C, to layer 3B from cells in middle depth and to layer 4A from the deepest part of the layer.

no more than 200  $\mu\text{m}$  but spanning the whole depth of 4C $\beta$ . Single LGN-M axons terminating in layer 4C $\alpha$  have fields that can spread up to 1.5 mm along an ocular dominance stripe and up to three ocular dominance stripes (each approximately 400  $\mu\text{m}$  wide) in the other dimension. The ratio of mean field width of single P to M axon arbors is about 1:3 (Blasdel & Lund, 1983). Most single M axon terminal fields occupy almost the whole depth of 4C $\alpha$ , though terminals may become sparse in upper-most 4C $\alpha$ . We have termed these M2 axons. Rare, large arbor M axons can be restricted in their terminal field to the top half of 4C $\alpha$  overlapping the upper half of the M2 fiber distribution (Blasdel & Lund, 1983, their figure 7; Freund, Martin, Soltesz, Somogyi & Whitteridge, 1989, see their Figure 1A but note that the boundary between 4C $\alpha$  and 4C $\beta$  is placed too high in this Figure—T. Freund, personal communication). We have called them M1 axons. Upper 4C $\alpha$  is characterized by a band of heavily myelinated, horizontally oriented, large diameter fibers which may partially correspond to these largest thalamic axons (Lund, 1973).

Within layer 4C, excitatory spiny stellate neurons constitute approximately 80% of the total cell population in the layer and are the major post-synaptic targets of LGN axon terminals. There is a gradual increase in cell density from 4C $\alpha$  to 4C $\beta$ ; the ratio of total number of 4C $\alpha$  cells to that of 4C $\beta$  cells is about 3:5 (O’Kusky & Colonnier, 1982) which is invariant with eccentricity (Livingstone & Hubel, 1988). Cortical cells in layer 4C are about 50–100 times more numerous than LGN cells (Chow, Blum & Blum, 1950; Peters, Payne & Budd, 1994); but while we have created realistic lateral overlap factors in cortical space for thalamic fiber arbors, we have not attempted to replicate realistically the cortical cell density since it does not bear on the results of this particular model.

Throughout the depth of the layer, the spiny stellate cells have their dendrites heavily overlapping one another (Fig. 1). While P axon terminals occupy only 4C $\beta$ , cells in the lower part of 4C $\alpha$  have dendritic intrusion into the 4C $\beta$  division, and we suggest that LGN-P axons would therefore also contribute inputs to these lower 4C $\alpha$  cells. Similarly, neurons in upper 4C $\beta$  have dendrites extending into M axon territory, and therefore these neurons should also receive some LGN-M-inputs. A related important observation is that the total number of excitatory spine synapses per spiny stellate neuron is approximately constant through the depth of layer 4C (Lund & Holbach, 1991; Peters, Payne & Budd, 1994).

While geniculocortical synapses account for only about 5–19% of total excitatory synapses on spiny stellate neurons in layer 4C (Peters, Payne & Budd, 1994; Anderson, Douglas, Martin & Nelson, 1994) they do appear to provide a reliable and potent drive to

these cells (Stratford, Tarczyhornocho Martin & Jack, 1996); the rest of the excitatory terminals are derived from recurrent axon collaterals of layer six pyramidal neurons (Anderson, Douglas, Martin & Nelson, 1994), intralaminar local projections from other layer 4C spiny stellate neurons (Fitzpatrick, Lund & Blasdel, 1985) and a light subcortical input from the claustrum (Carey, Bear & Diamond, 1980; LeVay & Sherk, 1981). Despite the presence of these other inputs, we make the assumption (important to our model) that the total number of geniculocortical synapses per spiny stellate neuron is constant throughout the depth of layer 4C. Taking this assumption together with the fact that dendritic overlap of spiny stellate neurons occurs through the depth of layer 4C, we postulate that layer 4C cells receive different numerical proportions of synapses from the LGN-M and -P afferent sets to make up their constant proportion of LGN-inputs. The proportion of M to P terminals depends on the position of the cell in the depth of the layer.

The axons of the LGN-M and -P cell populations are heavily overlapped laterally within their respective  $\alpha$  and  $\beta$  territories of layer 4C; this suggests that any single postsynaptic spiny stellate cell has a dendritic field receiving input from many laterally overlapped axon fields. The dendrites of single spiny stellate neurons are of much the same length and richness for single cells through the depth of the layer. However, the overall orientation of the dendritic field of single neurons changes through the layer from a slight emphasis on vertical extent for neurons in the  $\beta$  division to an emphasis on horizontal stratification in upper 4C $\alpha$ . The lateral spread of the dendritic arbor is however close to 200  $\mu\text{m}$  for single cells at any depth in layer 4C (Lund, 1980).

## 2.2. Overview of relevant physiological findings

Physiological studies of the macaque monkey show the P and M cells in the LGN at any given eccentricity to differ in their mean receptive field size, contrast sensitivity, and maximum firing rate. As first shown by Kaplan & Shapley (1982), M cells’ firing rates typically exceed those of P cells at each contrast level of stimulation. Fig. 2a, adapted from Derrington & Lennie (1984), shows that at each contrast level of visual stimulation, M cells’ firing rates typically exceed those of P cells. Fig. 2a shows that the contrast sensitivity for P cells is lower than that of M cells, where contrast sensitivity is typically defined as the reciprocal of the contrast level which can elicit criterion responses in the cells. Fig. 2b shows the contrast sensitivity versus spatial frequency tuning curves for a typical M cell and a typical P cell in the LGN. As the M cell has a lower peak spatial frequency, it can be inferred that the receptive field centre size of the M cell is larger than

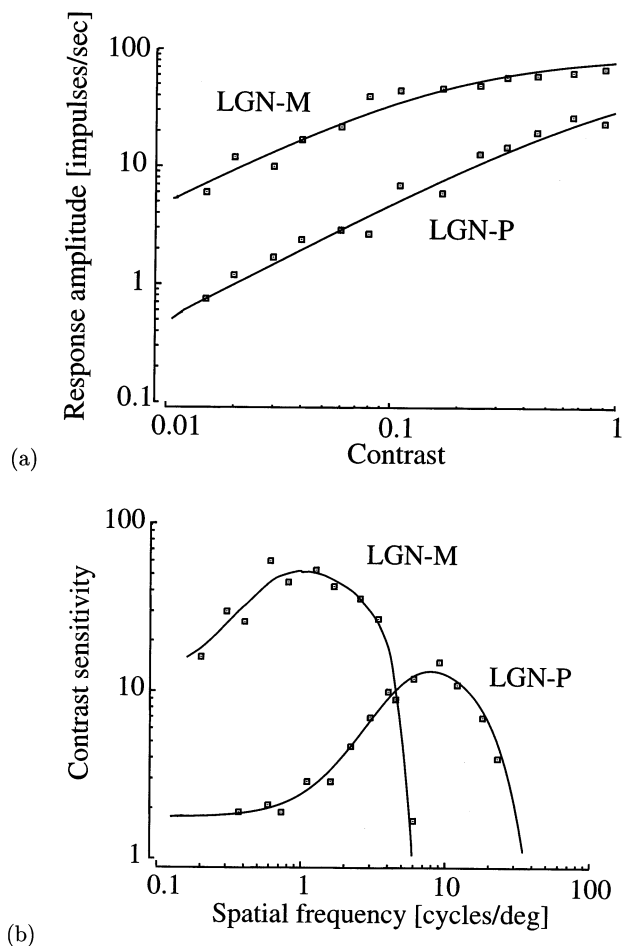


Fig. 2. (a) Response versus contrast curves for a typical LGN-M cell and a typical LGN-P cell; adapted from Derrington & Lennie (1984). Smooth curves drawn through the points are best-fitting solutions of a Michaelis–Menten function (Naka & Rushton, 1966). Reflected in this data is the fact that P and M neurons have different mean response characteristics in terms of maximum firing rate and contrast sensitivity—if defined as the reciprocal of the contrast level which would elicit a criterion response. (b) Contrast sensitivity versus spatial frequency curves for a typical LGN-M cell and a typical LGN-P cell; also adapted from Derrington & Lennie (1984). Smooth curves drawn through the points are best-fitting solution of a difference-of-gaussians function.

that of the P cell centre. The receptive field size of M cells is on average two to three times larger than that of P cells at any particular eccentricity across the visual field representation, although there is considerable variation as well as overlap in the receptive field size of both populations (Hicks, Lee & Vidyasagar, 1983; Derrington & Lennie, 1984; Spear, Moore, Kim, Xue & Tumosa, 1994). Similar results using various measurement techniques have also been obtained by many other investigators (e.g. Shapley, 1990).

Blasdel & Fitzpatrick (1984) and Hawken & Parker (1984) recorded from cells in layer 4C while making tangential electrode penetrations through the depth of V1. Blasdel & Fitzpatrick measured both receptive field

size and achromatic contrast sensitivity for a population of non-oriented cells; they used small slit or spot stimuli to determine a minimum response field for each cell. The cell's contrast threshold was then measured by using stimuli fitted to the cell's receptive field center and by gradually changing the contrast of the stimuli. Hawken & Parker used drifting sine-wave gratings to measure achromatic contrast sensitivity for a group of cells most of them classified as being orientation selective or orientation-biased. Though the absolute values of contrast sensitivity as measured in the two studies differ, reflecting the different measurement techniques, the changing trends as a function of depth in layer 4C are compatible. Two noticeable features are that there is a gradual decrease in receptive field size and contrast sensitivity in the cells recorded from top to bottom of layer 4C, and that the rate of decrease is much more rapid through the upper half of layer 4C $\alpha$  than through the rest of layer 4C, particularly for contrast sensitivity. Since both sets of data show similar trends, despite differences in absolute sensitivity values, we combined them in one representation. The data of Blasdel & Fitzpatrick were readily converted to the reciprocal contrast representation used by Hawken & Parker. Since the absolute sensitivity values of both studies were not comparable we scaled them to the mean value of each sample thus obtaining normalized contrast sensitivities. The re-analysed contrast sensitivities are shown in Fig. 3a. The receptive field sizes which are shown in Fig. 3b are exclusively from the data of Blasdel & Fitzpatrick (1984) since Hawken & Parker (1984) did not measure them. We interpret the data as exponential looking gradients for field size and contrast sensitivity through depth of layer 4C. In both plots of Fig. 3 we have divided the depth of layer 4C into eight equally sized intervals and calculated the mean value and standard deviation of the single unit measures falling in each depth interval. Since there is considerable scatter in the experimental data we use the statistical representations (solid curves in Fig. 3) as the data that should be matched in our simulated layer 4C neuron outputs.

In our second model we have anatomically classified LGN-M cells into two sub-groups (M1 and M2); possible physiological counterparts of the M1 axons, tentatively identified anatomically as terminating in the upper part of layer 4C $\alpha$ , are the data reported by Bullier & Henry (1980), when their boundary positions for layers 4B, 4C $\alpha$ , and 4C $\beta$  are corrected to conform with CO staining (compare their nissl stained cytoarchitecture boundaries with the CO boundaries of Blasdel & Lund, 1983; Fitzpatrick, Lund & Blasdel, 1985). With corrected boundaries, the units they report as having shortest latency input lie in upper 4C $\alpha$  (not in layer 4B), medium latency input occurs to cells of middle depth in 4C, and slowest latency is seen in the

lower half of 4C $\beta$ . Nowak, Munk, Girard & Bullier (1995) used the same cytoarchitectural boundaries as Bullier & Henry and so it is very likely that their fast thalamic inputs lie in layer 4C $\alpha$  rather than in 4B as reported but they do not provide a precise plot of latency in cortical depth. Maunsell & Gibson (1992) recorded multiunit latencies in depth of V1 in alert monkeys; we believe by comparison to proportional depth measures compared to CO stained V1 that layer 4C lies between  $-0.1$  and  $+0.3$  in the plot of all units in their Figure 12 and that in this case the shortest latencies occurred in the upper 2/5th of layer 4C.

### 2.3. Extrapolations from comparison of anatomical and physiological findings

The model hypothesis is that the functional gradient for contrast sensitivity and field size in layer 4C is derived from a changing ratio of M- versus P-inputs on

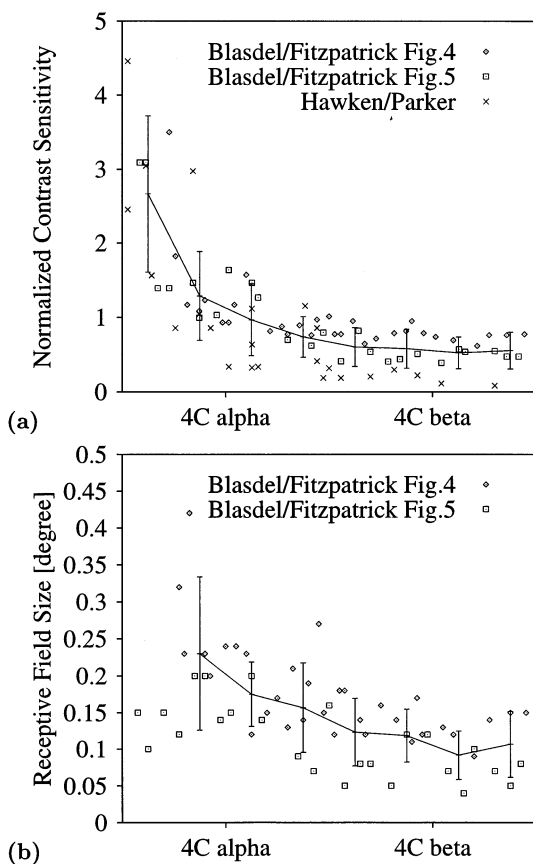


Fig. 3. Basic response properties of layer 4C spiny stellate neurons. The solid line in each panel intersect mean values ( $\pm$  standard deviations) at eight equally sized depth intervals through layer 4C. (a) Normalized contrast sensitivity of layer 4C spiny stellates (see text); plots are combined for the results of Blasdel & Fitzpatrick (1984), Hawken & Parker (1984). (b) Minimum response field (diameter) of layer 4C spiny stellate neurons as reported in the study of Blasdel & Fitzpatrick (1984). Since there are only two receptive field size measures falling in the interval at the top of layer 4C $\alpha$ , it is impossible to give a reliable expectation in this region.

Table 1  
Anatomical findings and magnification data used in this study

Property	Value	Source
LGN magnification factor	300 $\mu$ m/degree	Connolly & van Essen, 1984
Cortical magnification factor	1500 $\mu$ m/degree	Van Essen, Newsome & Maunsell, 1984
No. of LGN-P to no. of LGN-Mcells	6:1	Livingstone & Hubel, 1988
LGN-P axonal arbor	200 $\mu$ m ( $n = 32$ ) <sup>a</sup>	Blasdel & Lund, 1983 Freund, Martin, Soltesz, Somogyi & Whitteridge, 1989
LGN-M2 axonal arbor	600 $\mu$ m ( $n = 10$ ) <sup>a</sup>	
LGN-M1 axonal arbor	1100 $\mu$ m ( $n = 3$ ) <sup>b</sup>	
4C spiny stellate dendritic arbor	200 $\mu$ m ( $n = 25$ )	Lund, 1980

All parameters are taken from adult macaque monkeys and correspond to 5–8° eccentricity. The ratio of LGN-M2 to LGN-M1 cells was taken to be 7:1 if not mentioned otherwise. The numbers given in brackets indicate the sample size on which axonal and dendritic arbor sizes are based.

<sup>a</sup>  $n$  from Blasdel & Lund (1983).

<sup>b</sup>  $n$  from both Blasdel & Lund (1983) and Freund, Martin, Soltesz, Somogyi & Whitteridge (1989).

spiny stellate neurons at different depths in the 4C layer. As the position of spiny stellate neurons in layer 4C shifts from the very top of the layer to its base, they change the degree of their dendritic overlap into the terminal zones of M and P axons, and therefore we suggest that the relative weights of these thalamic inputs change accordingly. The combination of sets of physiologically distinct inputs to create a vertical functional gradient is of considerable importance to understanding the properties of the relays shown anatomically to emerge from layer 4C and which feed information to different sets of neurons providing extrinsic relays from the region.

## 3. Methods

### 3.1. Anatomical and physiological parameters

Table 1 summarises the known anatomical data on which our modelling study is based, together with its sources. The data are taken from adult macaque monkeys from a region in the visual field at eccentricity 5–8°.

Table 2 shows the corresponding physiological data for which two sets of data were used. The data set by Spear, Moore, Kim, Xue & Tumosa (1994) was taken

from macaque LGN P- and M-layers but mostly mean values were reported which were averaged over different animals and over a range of eccentricities from 0 to 10°, together with the corresponding standard deviations. The data set by Croner & Kaplan (1995) provides a large sample of cells, but the data were collected from retinal P and M ganglion cells rather than their geniculate counterparts. As Croner & Kaplan note, however, differences in these physiological properties between the retinal and the geniculate populations is small.

None of these studies distinguish between two populations of geniculate M cells, but it is reasonable to assume that M1 cells have larger receptive fields: Sclar, Maunsell & Lennie (1990) report that increase in field size is accompanied by increase in contrast sensitivity along the visual path from LGN to area MT, thus larger fields imply higher contrast sensitivities. Therefore we hypothesize that LGN-M1 cells correspond to the upper fraction of the LGN-M population with respect to contrast sensitivity and receptive field size and we study the effect of varying the ratio between LGN-M1 and LGN-M2 cells in Sections 4.2.2 and 4.2.3.

Center ( $R_c$ ), surround ( $R_s$ ) radii, and the ratio  $K = (K_s * R_s^2) / (K_c * R_c^2)$  of the integrated surround/center sensitivities are drawn independently from normal distributions given by the mean values and standard deviations of Tables 2 and 3. Although the different receptive field parameters may be correlated and the distribution of parameter values may be skewed, there are not sufficient experimental data available to estimate the corresponding parameters and to infer more complicated distributions.

### 3.2. Neural network architecture

Our model consists of three sets of layers, which correspond to the visual field, the LGN and cortical layer 4C (Fig. 4). The visual field layer is used to present the grating, bar and spot stimuli. Each geniculate layer corresponds to a different population of geniculate cells, hence there are two layers for the P- and M-, and three layers for the P-, M2- and M1 populations of the corresponding versions of the network model. Layer 4C consists of eight sublayers, four for the  $\alpha$  and  $\beta$  divisions, which correspond to eight different depths. The cells in each sublayer lie on quadratic grids of size  $N_S^{LGN} \times N_S^{LGN}$  and  $N_D^{4C} \times N_D^{4C}$ , where  $S \in \{P, M, M2, M1\}$  and  $D \in \{1, \dots, 8\}$ . The grid size of the LGN-P layer is chosen to ensure a receptive-field coverage factor of greater than 1 and the grid size of the LGN-M layer(s) is proportional to the densities of the M population (M or M2 + M1) relative to the P population. Since the ratio between the total number of layer 4C cells to the total number of geniculate cells is not critical to our model it was much less than 100:1. For computational reasons no realistic total cell numbers, neither in the LGN layers nor in cortical layer 4C are used, but the ratio of P to M (M2 + M1) cells (Table 1) and the ratio of 4C $\alpha$  to 4C $\beta$  neurons which is 3:5 (O'Kusky & Colonnier, 1982) match the experimental data. Layers are connected in a feedforward manner. Lateral and recurrent projections are ignored, because the purpose of this study is to single out the effect of the feedforward convergence of LGN afferents to spiny stellate neurons in layer 4C.

All neurons are modeled as continuous connectionist neurons, whose output values  $O_i$ ,

Table 2  
Physiological parameters of P and M cells

	Physiological parameters	Croner & Kaplan	Spear et al.
LGN-P	Center radius $R_c$	0.05 ± 0.03	0.087 ± 0.046
	Surround radius $R_s$	0.43 ± 0.28	0.53 ± 0.39
	Integrated surround-center sensitivity $K$	0.547 ± 0.181	—
	Contrast gain $G$	0.963 ± 0.483	0.66 ± 0.32
	Max. firing rate $M$	—	31.11 ± 11.32
LGN-M	Center radius $R_c$	0.10 ± 0.02	0.103 ± 0.021
	Surround radius $R_s$	0.72 ± 0.23	1.16 ± 0.48
	Integrated surround-center sensitivity $K$	0.546 ± 0.120	—
	Contrast gain $G$	5.896 ± 2.161	1.43 ± 0.87
	Max. firing rate $M$	—	45.05 ± 24.45

The table provides median ± interquartile range for the Croner & Kaplan (1995) data and mean values ± standard deviations for the data of Spear, Moore, Kim, Xue & Tumosa (1994). Radii are given in degrees of visual field, contrast gains are given in (spikes s<sup>-1</sup> % contrast<sup>-1</sup>), and neural responses are given in (spikes s<sup>-1</sup>). Although the Croner & Kaplan data are from retinal ganglion cells, we assume that the organization of receptive fields found in the LGN does not differ much from those of retinal ganglion cells, especially at eccentricities near the fovea. The integrated surround / center sensitivity  $K$  is defined as  $(K_s R_s^2) / (K_c R_c^2)$ . As reported in Croner & Kaplan the average ratio of surround/center sensitivity is constant across the visual field and equal for P and M cells. Since Croner & Kaplan (1995) do not report maximum firing rates of P and M cells we have used the values given in the study of Spear, Moore, Kim, Xue & Tumosa (1994).

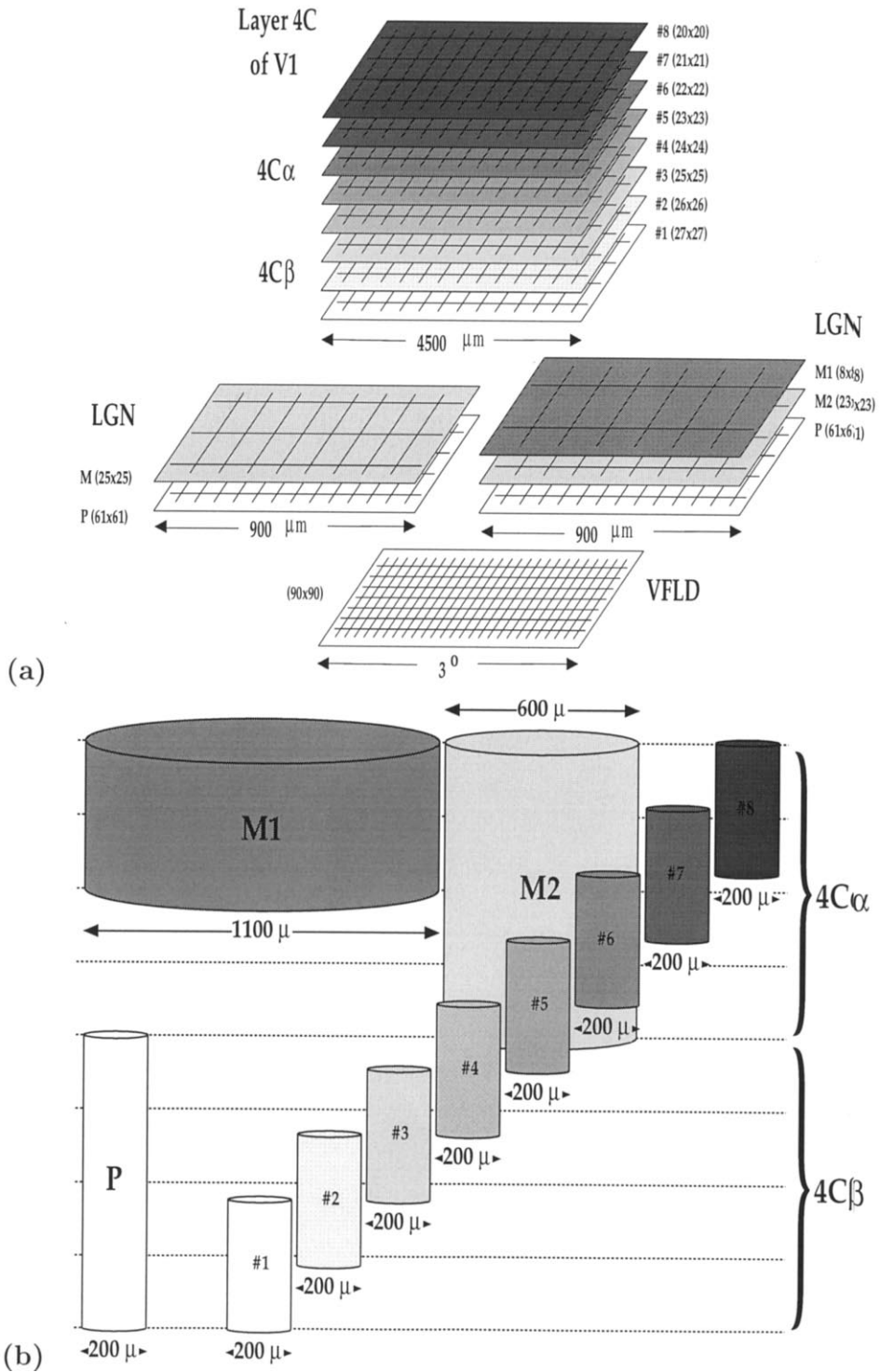


Fig. 4. (a) Neural network architecture. The model consists of three sets of layers. The visual field is represented by one, the LGN cell populations by either two (M and P, left) or three (M1, M2, and P, right) and layer 4C by eight sublayers (eight different depth values), four sublayers each for 4C  $\alpha$  and 4C  $\beta$ . The numbers denote grid sizes ( $N_x^L \times N_y^L$ ) and are—for the geniculate and the cortical layers—proportional to the cell number densities (taken from Livingstone & Hubel (1988), O’Kusky & Colonnier (1982)). A ratio of 3:5 for layer 4C  $\alpha$  to 4C  $\beta$  cells is adopted by linearly increasing the grid size from top to bottom of layer 4C. (b) Cartoon of afferent axon arbors in comparison with spiny stellate dendritic fields. Numbers indicate lateral spread. P axon arbors project to the  $\beta$ , M (M2) arbors to the  $\alpha$  sublayers respectively. M1 arbors are restricted to the top half of 4C  $\alpha$ . Width and height of spiny stellate dendritic arbors is assumed to be approximately independent of depth (but see Section 4.1.3 for numerical simulations with varying dendritic arbor parameters). The figure is a summary of data from Lund (1980).

Table 3  
Four sets of physiological parameters of LGN-M2 and LGN-M1 cells

(a) Receptive field size		Set A	Set B	Set C	Set D
LGN-M2	$R_c$	$0.097 \pm 0.02$	$0.096 \pm 0.019$	$0.094 \pm 0.019$	$0.093 \pm 0.018$
	$R_s$	$0.72 \pm 0.21$	$0.71 \pm 0.21$	$0.70 \pm 0.20$	$0.69 \pm 0.20$
LGN-M1	$R_c$	$0.103 \pm 0.022$	$0.110 \pm 0.021$	$0.116 \pm 0.025$	$0.121 \pm 0.026$
	$R_s$	$0.75 \pm 0.21$	$0.84 \pm 0.24$	$0.93 \pm 0.24$	$0.98 \pm 0.25$
M2:M1 (%)		59:41	72:28	80:20	88:12
(b) Contrast processing		Set A	Set B	Set C	Set D
LGN-M2	G	$5.711 \pm 1.974$	$5.599 \pm 1.877$	$5.472 \pm 1.791$	$5.313 \pm 1.899$
	M	$44.58 \pm 19.90$	$43.46 \pm 18.46$	$43.07 \pm 17.82$	$41.65 \pm 16.76$
LGN-M1	G	$6.270 \pm 1.899$	$6.920 \pm 1.811$	$7.899 \pm 1.383$	$8.806 \pm 0.988$
	M	$56.23 \pm 21.14$	$66.06 \pm 19.96$	$70.28 \pm 20.37$	$79.32 \pm 23.43$
M2:M1 (%)		59:41	72:28	80:20	88:12

Note that number ratio of LGN-M2 and LGN-M1 cells for corresponding sets in both tables are identical. (a) Four sets of receptive field sizes and number densities (last row) of LGN-M2 and LGN-M1 cells used in this study ( $R_c$  = center radius;  $R_s$  = surround radius). Mean values and standard deviations of center and surround radii are given in degrees visual field. The mean values and standard deviations for the total LGN-M population,  $R_c = 0.10 \pm 0.02$  and  $R_s = 0.72 \pm 0.23$  (Croner & Kaplan, 1995) are constant over all sets. Note further, that the value of the integrated surround/center sensitivity  $K$  is independent of the specific cell population ( $0.55 \pm 0.12$ ); therefore  $K$  remained constant for all parameter sets. (b) Four sets of contrast gains ( $G$ ) and maximum spike rates ( $M$ ) for LGN-M2 and LGN-M1 cells used in this study. Number densities of LGN-M2 and LGN-M1 cells are given in the last row. Mean values and standard deviations of contrast gains and maximum spike rates are given in (spikes  $s^{-1}$  % contrast $^{-1}$ ) and (spikes  $s^{-1}$ ), respectively. The maximum spike rates are taken from the data set of Spear et al. since Croner & Kaplan do not report them. The mean values and standard deviations for the total LGN-M population,  $G = 5.896 \pm 2.161$  and  $M = 45.05 \pm 24.45$  (Croner & Kaplan, 1995; Spear, Moore, Kim, Xue & Tumosa, 1994), are constant over all sets.

$$O_i = f(I_i), \quad I_i = \sum_j w_{ij} O_j \quad (1)$$

denote the cells' firing rates.  $I_j$  is the total input of neuron  $j$ ,  $w_{ij}$  the weight of the connection between neurons  $j$  and  $i$ , and  $f$  is a sigmoid transfer function which is specific to each population of cells.

### 3.3. Visual stimulation

Stimuli are coded by the activity  $O(x, y)$  of the units at positions  $(x, y)$  in the visual field layer. We used:  
—Spots of radius  $r$  and contrast  $c$  at position  $(x_m, y_m)$  in the visual field:

$$O(x, y) = \begin{cases} l_0(c + 1) & \text{if } (x - x_m)^2 + (y - y_m)^2 \leq r^2 \\ l_0 & \text{otherwise} \end{cases} \quad (2)$$

—Bars of size  $(d_x, d_y)$ , orientation  $a \in ]0, \pi]$ , contrast  $c$  at position  $(x_m, y_m)$  in the visual field:

$$O(x, y) = \begin{cases} l_0(c + 1) & \text{if } |(x - x_m)\cos a + (y - y_m)\sin a| \\ & \leq 0.5d_x \text{ and } |-(x - x_m)\sin a + (y - y_m)\cos a| \leq 0.5d_y \\ l_0 & \text{otherwise} \end{cases} \quad (3)$$

—Sine wave gratings of variable spatial frequency  $v$ , contrast  $c$  and phase defined by

$$O(x, y) = l_0 + cl_0 \sin(2\pi vx + \phi) \quad (4)$$

Stimulus contrast is given by  $c = (l_p - l_0) l_0^{-1}$  where  $l_p$  denotes the luminance of the spot, the bar or the maximum luminance of the sine wave grating, and  $l_0$  is the luminance of the background or the mean luminance.

### 3.4. LGN neurons

#### 3.4.1. Receptive fields

The response properties of the LGN cells are modeled by a Difference-of-Gaussians (DoG) model (Rodieck, 1965; Enroth-Cugell & Robson, 1966; Linsenmeier, Frishman, Jakiela & Enroth-Cugell, 1982). The corresponding weights  $w_{ij}$  are given by:

$$w_{ij} = \frac{1}{2\pi R_{c_i}} e^{-1/(R_{c_i})^2[(x_j - x_i)^2 + (y_j + y_i)^2]} - \frac{K_i}{2\pi R_{s_i}} e^{-1/(R_{s_i})^2[(x_j - x_i)^2 + (y_j - y_i)^2]} \quad (5)$$

$R_{c_i}$  and  $R_{s_i}$  denote the center and surround radii,  $K_i$  the integrated surround/center sensitivity and  $(x_i, y_i)$  the position of the receptive field center of the geniculate neuron  $i$  in visual space.  $(x_j, y_j)$  is the position of a unit  $j$  in the visual field layer. To save computation time, weights were set to zero outside a circular region of radius  $2R_{s_i}$ .

### 3.4.2. Transfer functions

Transfer functions are rectified sigmoid functions

$$f_{\beta}^{\text{LGN}}(x) = \max\left(p_0 \frac{1 - e^{-p_1(x - p_2)}}{1 + e^{-p_1(x - p_2)}} + p_3, 0\right) \quad (6)$$

parameterized by the maximum spike rate  $p_0$ , the gain  $p_1$  and the horizontal and vertical offsets  $p_2$  and  $p_3$ . In the following we consider transfer functions of type 1 ( $p_3 \approx 0$ ) and transfer functions of type 2 ( $p_3 = 0.5 p_0$ ). Contrast response functions are usually described by a Michaelis-Menten relationship (Naka & Rushton, 1966)

$$r_i(c) = \frac{M_i c}{C_i + c} \quad (7)$$

where  $r_i$  is the response of cell  $i$ ,  $c$  denotes the % contrast of an optimal sine wave grating,  $M_i$  is the maximum response and  $C_i$  is the % contrast at which the response has reached 50% of its maximum (semi-saturation). The contrast gain  $G$  of a geniculate cell is defined as the slope of the initial rising phase of the response versus contrast function (see Spear, Moore, Kim, Xue & Tumosa, 1994; Croner & Kaplan, 1995). It therefore directly follows that the semi-saturation contrast is related to the contrast gain  $G_i$  via  $C_i = M_i(G_i)^{-1}$ . Contrast gain, maximum response and receptive field parameters were randomly assigned to each LGN neuron according to the normal distributions with parameters given in Tables 2 and 3.

The parameters  $p_0 \dots p_2$  of the type 1 transfer function were subsequently determined via a least squares fit of the model predictions—Eqs. (1) and (4) and Eq. (5) for sine wave gratings of optimal spatial frequency—to the actual response given by Eq. (7). If not explicitly mentioned in the text, transfer functions of type 1 are used.

Type 2 transfer functions are used only in one special case and only for model LGN-P cells (see Section 4.1.2) to account for differences in the response of geniculate P- and M-cells to low contrast stimuli (Spear, Moore, Kim, Xue & Tumosa, 1994; Livingstone & Hubel, 1987).

The parameters  $p_0 \dots p_2$  of the type 2 transfer function were determined in the same way as described above, but with the following exception: to obtain a realistic fit for low contrast stimuli, the actual response was given by  $r_i(c) = M_i (c - c_{\min}) / (C_i + c - c_{\min})^{-1}$ , where  $c_{\min}$  denotes the contrast threshold of the geniculate cell. Because we are seeking to explain the nonlinearity in the gradient of basic response properties in depth of layer 4C, it was necessary to test whether the difference in low contrast processing between P- and M-cells could affect the shape of the curves in a qualitative way, i.e. induce symmetry breaking at the top of layer 4C $\alpha$ . Therefore we chose an extreme value for the contrast threshold of P cells ( $c_{\min} = 10\%$  taken from Livingstone & Hubel (1987)).

### 3.5. Cortical neurons

#### 3.5.1. Geniculocortical connectivity

Fig. 4b shows a cartoon of the afferent axon arbors in comparison with spiny stellate dendritic fields in layer 4C. P and M (M2) axon arbors project to the full  $\beta$  and  $\alpha$  sublayers respectively; M1 arbors are restricted to the top of 4C $\alpha$ . Width and height of spiny stellate dendritic arbors are assumed to be approximately independent of depth (but see Section 4.1.3).

The weight  $w_{ij}$  of the connection between a geniculate cell  $j$  of population  $S$  and a cortical cell  $i$  in layer  $D$  is calculated via the two-dimensional areal overlap  $a_{ij}$  between the circular cross-sections of the corresponding axonal and dendritic arbors. The areal overlap  $a_{ij}$  can be derived from the anatomical parameters (see Fig. 4b and Table 1).

The weight  $w_{ij}$  of a geniculate cell of population  $S$  also scales with the vertical overlap of cylinders in depth  $D$  of layer 4C. This is indicated by the different heights and locations of cylinders in depth  $D$  (see Fig. 4b).

Because it is the overlap in depth of layer 4C which is crucial to our model we have introduced a separate set of parameters. The layer specificity of afferent termination and dendritic sampling zones is taken into account by the thalamic weight portion  $W^{\text{LGN}-S}(D)$  which denotes the probability that a spiny stellate neuron receives a synaptic contact from a cell of the geniculate subpopulation  $S$ . Thus the thalamic weight portions for depth  $D$  of layer 4C satisfy the constraint

$$\sum_S W^{\text{LGN}-S}(D) = 1 \quad (8)$$

Since the number of spines is fairly constant for each spiny stellate cell  $i$  and a constant percentage of spines is occupied by thalamic axon terminals, we determined synaptic weights  $w_{ij}$  by normalizing

$$w_{ij} = \frac{W^{\text{LGN}-S}(D)}{\sum_j a_{ij}} \quad (9)$$

The change of the quantities  $W^{\text{LGN}-S}(D)$  with depth must be consistent with the overall anatomical data i.e. there should be a linear transition from P- to M-input with rise in depth of layer 4C (see Fig. 4b). Nevertheless the numerical values cannot be derived from the data. In order to explore the influence of thalamic weight portions on receptive field sizes and contrast sensitivities we have tested different thalamic weight distributions (see Section 4).

#### 3.5.2. Measurement of receptive field size and contrast sensitivity

Receptive field size and contrast sensitivity are calculated as described in Blasdel & Fitzpatrick (1984): A

small bar of low contrast, Eq. (3) with  $d_x = 0.03^\circ$ ,  $d_y = 0.3^\circ$  and  $c = 20\%$ , is systematically moved along each of eight directions  $l = \pi/4, \pi/2, \dots, 2\pi$  from the center towards the border of the receptive field. The angle  $a$  of the bar in Eq. (3) was chosen perpendicular to the orientation of movement. The average distance  $r^i$  at which the total input  $I_i$  (see Eq. (1)) of the cortical cell  $i$  falls below a given threshold  $t_0$  is interpreted as the radius of the receptive field. Subsequently a spot of radius  $r^i$  is fitted to the individual minimum response field, and its contrast is increased until the cell's input  $I_i$  reaches another fixed threshold  $t_1$ . Contrast sensitivity is then defined as the reciprocal threshold contrast for the corresponding total input  $t_1$ . Contrast sensitivities curves are normalized to the average contrast sensitivity of the total sample in order to allow a comparison with data (for details refer to Section 2.1).

## 4. Results

In the following we consider both neural network architectures of Fig. 4 which we call model I (one M population) and model II (two M populations), and we systematically explore their parameter spaces. Both data sets, Spear, Moore, Kim, Xue & Tumosa (1994), Croner & Kaplan (1995), were used to estimate the parameters of geniculate neurons, but numerical simu-

lations lead to virtually identical conclusions. Therefore, in most cases we present only the results for the Croner & Kaplan data. Variations of cortical threshold parameters  $t_0$  and  $t_1$  over a considerable large range ( $t_0 = 0.5-3.0$  and  $t_1 = 5.0-15.0$ ) lead to different absolute values of receptive field size and contrast sensitivity curves, but leave the shape of both curves unchanged.

### 4.1. Model I: one LGN-M population

#### 4.1.1. Percentage of P- versus M-inputs as a function of depth

We performed numerical simulations for the four sets of thalamic weight portions  $W^{\text{LGN-P}}(D)$  and  $W^{\text{LGN-M}}(D)$  shown in Fig. 5. The predicted receptive field sizes and contrast sensitivities are summarized in Fig. 6a. The overall shape of the curves changes from a step function for segregated inputs to an almost linear function in the case of heavily convergent thalamic input. As the degree of convergence increases, the curves become smoother and the flat plateaus at the top and bottom of layer 4C which resemble pure LGN-M and LGN-P properties become less significant. Note that none of the curves shows the dramatic increase of contrast sensitivity in upper 4C $\alpha$  seen in the experimental data. A good match, however, is obtained for lower 4C $\beta$  and mid-4C for the weight distribution of Fig. 5c, which is the biologically most realistic given the

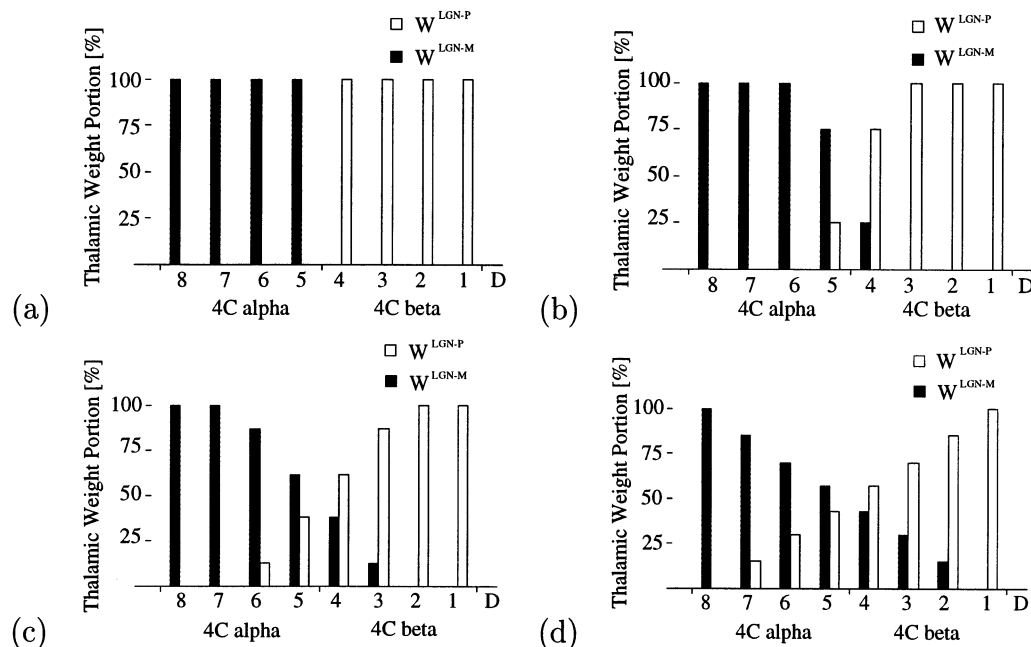


Fig. 5. Proportion of P- and M-inputs to spiny stellate cells as a function of depth in model layer 4C. Each plot shows the thalamic weight portions  $W^{\text{LGN-P}}(D)$  and  $W^{\text{LGN-M}}(D)$  at eight discrete depths of layer 4C. (a) Full segregation of P- and M-inputs. (b) Small zone of convergence at the border between layers 4C $\alpha$  and 4C $\beta$  ( $D = 4, 5$ ). (c) Spiny stellate neurons deeper in the  $\beta$  and  $\alpha$  divisions (up to sublayer  $D = 3, 6$ ) are allowed to listen to both types of incoming afferents. (d) Spiny stellate neurons at almost every depth of layer 4C (up to sublayers  $D = 2, 7$ ) make intrusions into the termination zones of both pathways. The weight distribution (c) corresponds to the cartoon in Fig. 4b and thus represents the proportional overlap of dendritic and axonal fields in depth of layer 4C as observed anatomically. It results in the best fit of simulated and real physiological data in depth of layer 4C and it is furthermore the most plausible configuration in terms of anatomical evidence.

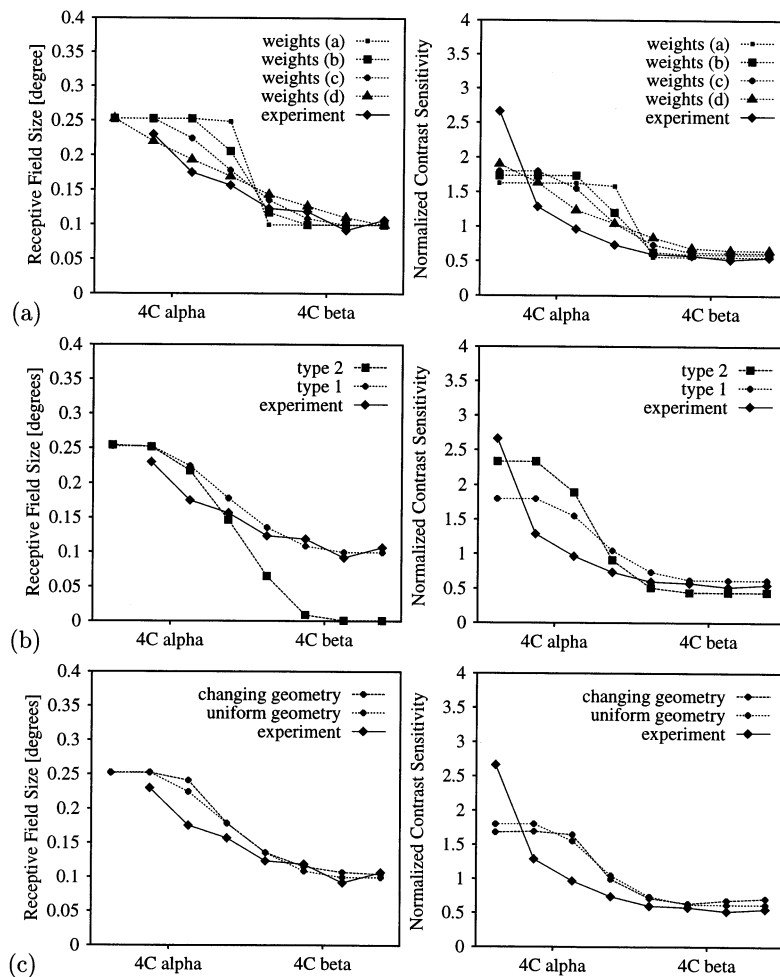


Fig. 6. Parameter exploration of model I (one M pathway). The figure shows receptive field size (left column) and contrast sensitivity (right column) of layer 4C spiny stellate neurons as a function of depth  $D$ ,  $D = 1, \dots, 8$ . Symbols denote mean values of 20 cells selected at random from each sublayer. Each curve corresponds to a particular choice of model parameters; plots of the experimental data from Fig. 3 are added for comparison. Threshold parameters were  $t_0 = 2.45$  and  $t_1 = 13.75$ . (a) Convergence of P- and M-inputs: Each curve refers to the corresponding thalamic weight distribution of Fig. 5. (b) Plots of response properties for type 1 versus type 2 LGN-P transfer functions. The thalamic weight distribution was taken from Fig. 5(c). The higher normalized contrast sensitivity at the top of layer 4C $\alpha$  in the type 2 versus the type 1 curve is an artefact of normalization; the absolute contrast sensitivities at the top of layer 4C $\alpha$  are equal for both type 2 and type 1 simulations. (c) Effect of changes in the dendritic arbor geometry of the spiny stellate neurons. The lateral spread of the dendritic fields changed from  $150 \mu\text{m}$  at the bottom to  $250 \mu\text{m}$  at the top of layer 4C. The thalamic weight distribution of Fig. 5c was adapted to account for the vertical versus horizontal elongation of the dendritic fields at the bottom and top of layer 4C. The response properties for spiny stellate cells with uniform dendritic field geometry are also shown (compare plot (a), weights (c)).

anatomical findings. This set of weights is used as a baseline for further modeling steps.

#### 4.1.2. Transfer functions of geniculate P-cells

We seek to explain the nonlinear gradients of basic response properties in depth of layer 4C. Therefore it was necessary to test, if differential processing of low contrast stimuli of the P- and M-cells could affect receptive field size and contrast sensitivity of cortical cells in a qualitative way, i.e. could induce symmetry breaking in depth of layer 4C. Therefore, for simulation results discussed in this section, a type 2 transfer function was chosen for model P-cells (Section 3.4.2).

Fig. 6b shows the effect of the type 1 and 2 transfer functions when applied to geniculate P cells. Given the fact, that type 2 transfer functions lead to model P cells which remain basically silent below contrast values of 10%, it is not surprising that the differences in contrast sensitivity and receptive field size between cells in lower 4C $\beta$  and upper 4C $\alpha$  become more pronounced and that the region of strongest increase of receptive field size is shifted into 4C $\beta$ . Without normalization of the simulation data a similar shift into 4C $\beta$  is also apparent for the contrast sensitivity curve. Unfortunately this observation is obscured by the normalization procedure and thus a shift in the normalized contrast sensitivity curve in Fig. 6b is not clearly visible. The overall shape of the

curves remains sigmoidal, though, and the contrast sensitivity remains plateau-like in upper 4C $\alpha$ . Note that the higher values of the normalized contrast sensitivity at the top of layer 4C $\alpha$  in the type 2 curve is an artefact of normalization. The values of the absolute contrast sensitivity at the top of layer 4C $\alpha$  are equal for both type 2 and type 1 simulations.

#### 4.1.3. Dendritic arbor size of layer 4C spiny stellate neurons

So far we have assumed that the lateral and vertical spread of layer 4C spiny stellate neurons are independent of depth but anatomical findings suggest that spiny stellate dendritic arbors at the bottom of layer 4C are more strongly elongated in the vertical direction while dendrites of neurons at the top of layer 4C show an increased lateral spread (see also Section 2.2).

In order to study the effect of changing dendritic arbor geometry, dendritic fields of neurons at the bottom of layer 4C were allowed to reach into the termination zone of the M pathway while dendrites of upper 4C $\alpha$  neurons were confined to the 4C $\alpha$  subdivision. Also, lateral diameter of spread of the dendrites was assumed to change linearly from 150  $\mu\text{m}$  at the bottom of 4C to 250  $\mu\text{m}$  at the very top. The simulation results (Fig. 6c) still show curves of receptive field size and contrast sensitivity which saturate at the top of layer 4C similar to the other results shown in Fig. 6. Thus a more realistic model of dendritic field lateral spread is still not able to explain the exponential increase of contrast sensitivity at the top of layer 4C $\alpha$ .

## 4.2. Model II: two LGN-M populations

The numerical simulations of the previous section showed that model I is not able to produce a good fit to the data in upper 4C $\alpha$ , though it leads to reasonable results for the rest of 4C. In this section we, therefore, concentrate on the assumption of two LGN-M populations and explore parameter space of model II with focus on the upper 4C $\alpha$  region and on the properties of the postulated M1 and M2 afferents.

#### 4.2.1. Percentage of M1- versus M2-inputs as a function of depth

As already mentioned in the Section 2, it is reasonable to assume that M1 cells have larger receptive field size, contrast gain and maximum spike rates than the M2 cells (for details see Set D in Table 3a, b and the caption of Fig. 8).

Because the response properties of spiny stellate cells in lower 4C $\beta$  and mid-4C should not be affected by LGN-M1-input to upper 4C $\alpha$  we may use the distribution of synaptic contacts between the P- and the M-af-

ferents from Fig. 5c as a starting point and just split the weight portion  $W^{\text{LGN-M}}$  between the new subpopulations  $W^{\text{LGN-M1}}$  and  $W^{\text{LGN-M2}}$ . Fig. 7 shows four sets of thalamic weight portions with different degrees of M1–M2 convergence which were explored in numerical simulations.

Fig. 8a shows the corresponding predicted curves for receptive field size and contrast sensitivity. Both response properties are dramatically increased at the top of layer 4C $\alpha$  as soon as M1-input is present. The best match with the experimental data is obtained for the set of weights depicted in Fig. 7b, which is also consistent with the anatomical finding that LGN-M1 axon arbors are restricted to the top of layer 4C $\alpha$  with little intrusion of dendrites from cells in the lower parts of 4C $\alpha$ . This set of weights will be used as a starting point for further parameter explorations.

#### 4.2.2. Effects of receptive field size of LGN-M1 neurons

The physiological parameters of LGN-M1 versus LGN-M2 cells are hypothetical and cannot be fully constrained by data. In order to explore their influence on model predictions we consider the four sets of parameter values listed in Table 3a, b and we concentrate on receptive field parameters first.

The size of the LGN-M1 fields were increased from sets A to D of Table 3a such that the mean values and the standard deviations for the whole LGN-M population (LGN-M1 plus LGN-M2)—which had been measured experimentally by Croner & Kaplan (1995)—remained constant (see caption Fig. 3a). As a consequence, the mean receptive field sizes of the LGN-M2 population slightly decrease from sets A to D but—more important—the ratio of LGN-M1 to LGN-M2 cells also decreases: While LGN-M1 cells form the topmost 41% fraction of the LGN-M population for set A they occupy only the topmost 12% for set D. Contrast gains and maximum spike rates were taken from Table 2 and were—for the numerical simulations presented in this section—assumed to be identical for both M populations. The weight distribution was set according to Fig. 7b.

Fig. 8b shows the corresponding receptive field size and contrast sensitivity curves. The shape of the curves is almost identical for all four sets of parameters given in Table 3a, hence the changes in receptive field size of the LGN-M1 cells do not have a strong impact on the gradient of physiological properties in 4C. The fact that both populations of M-cells are now assigned similar contrast gain values leads to a drop of the contrast sensitivity in upper 4C $\alpha$  and to an increase in mid 4C when compared to Fig. 8a. This is to be expected, because the sensitivities (spikes  $\text{s}^{-1}$   $\% \text{contrast}^{-1} \text{deg}^{-2}$ ) were increased for the LGN-M2 cells, which dominate mid 4C-input, and decreased for the LGN-M1 cells, which dominate the input to upper 4C $\alpha$ .

Contrast sensitivity in upper 4C $\alpha$ , however, is even less than in mid 4C, although equal values were chosen for the contrast gains of LGN-M1 and LGN-M2 cells. This is also due to the larger receptive field area of the M1-cells at similar contrast gain which leads to a lower average sensitivity (spikes s<sup>-1</sup> % contrast<sup>-1</sup> deg<sup>-2</sup>).

4.2.3. Effects of contrast sensitivity of LGN-M2 and LGN-M1 neurons

From the results presented in the previous section it becomes clear that contrast sensitivity as well as receptive field size must differ between LGN-M1 and LGN-M2. Therefore, contrast gain values and maximum spike rates were now also increased, according to Table 3b. The weight distribution was set according to Fig. 7b and the physiological properties of LGN-P cells were taken from Table 2.

The results are shown in Fig. 8c. As differences in receptive field size and contrast sensitivity between LGN-M1 and LGN-M2 cells increase (Table 3a, b) both response properties increase for cells in upper 4C $\alpha$  and decrease for cells in mid 4C until the curves finally match the experimental data. A perfect match is achieved with parameter set D of Table 3a, b for which DoG parameters, contrast gains and maximum spike rates of the M1 cells are roughly one standard deviation above the mean value of the total LGN-M population.

4.3. Best predictions

So far only the results of simulations using the Croner & Kaplan data set have been presented, although parameter explorations were also performed for the Spear, Moore, Kim, Xue & Tumosa (1994) data set. To conclude our study, we summarize the optimal fits of mo2del II to the experimental data for both data sets (Spear, Moore, Kim, Xue & Tumosa, 1994; Croner & Kaplan, 1995), including error bars, in Fig. 9.

The experimental data match the model predictions obtained for both sets of data, but the optimal values for the free model parameters differ slightly as shown in Table 4. While the data of Croner & Kaplan suggest a ratio of M and P contrast gains of 5:1, the ratio for the Spear et al. data is only 3:1 (see Table 2). Therefore, the exponential change of response properties through depth of layer 4C $\alpha$  requires an onset of M1-input deeper in layer 4C $\alpha$  for the Spear et al. than for the Croner & Kaplan data. The model results indicate that M1-input cannot be confined to a sharp border in depth of layer 4C; in fact, intrusion of depth 6 spiny stellate cell dendrites into the upper half of layer 4C $\alpha$ , i.e. into M1 axon territory as predicted for the Spear et al. data (compare Table 4), is consistent with biological findings.

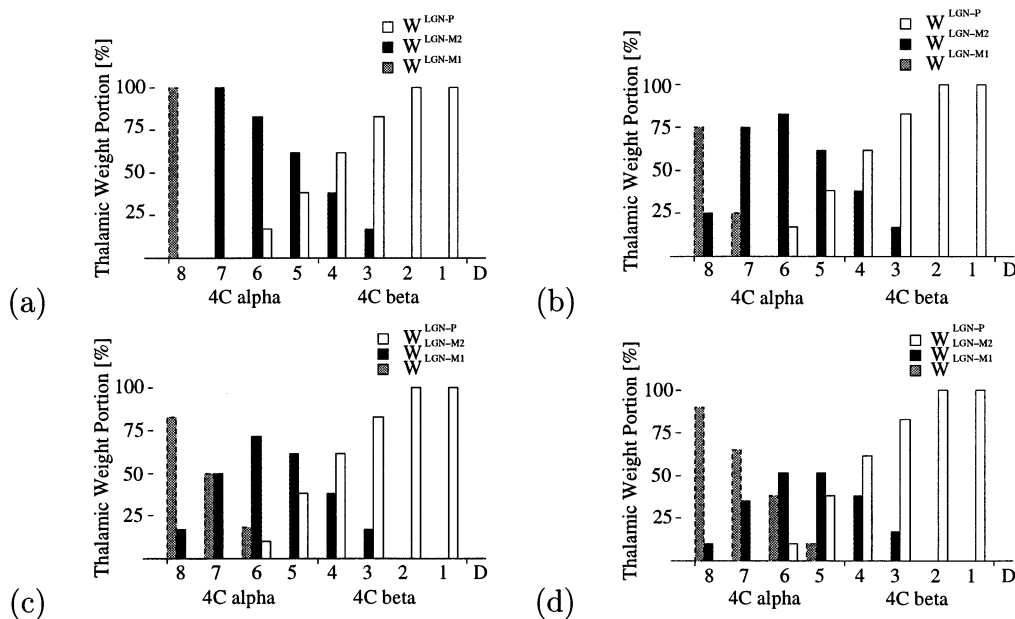


Fig. 7. Proportion of P-, M1- and M2-inputs to spiny stellate cells as a function of depth in model layer 4C. Each plot shows the thalamic weight portions  $W^{LGN-P}(D)$ ,  $W^{LGN-M1}(D)$  and  $W^{LGN-M2}(D)$  at eight discrete depths of layer 4C. The proportion of P- versus the total M-input was taken from model I (Fig. 5c). (a) Full segregation of M1- and M2-inputs. (b) Small zone of convergence of M1- and M2-inputs in upper 4C $\alpha$  ( $D = 7,8$ ). (c) M1 afferents now also project to sublayer  $D = 6$ . (d) All spiny stellate cells in layer 4C $\alpha$  sample from both LGN-M afferents. Since the sample of anatomically identified M1 cells is small it is not possible to decide if weight distribution (b) or (c) is the most plausible configuration in terms of anatomical evidence (see also Section 4.3).

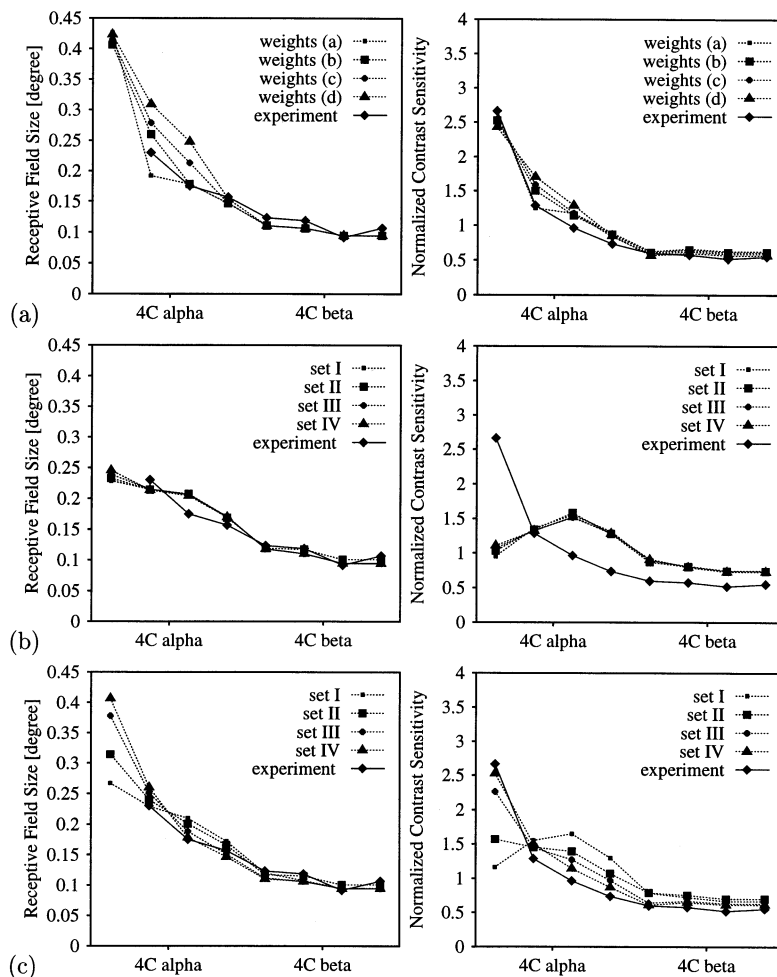


Fig. 8. Parameter exploration of model II (two M pathways). The figure shows receptive field size (left column) and contrast sensitivity (right column) of layer 4C spiny stellate neurons as a function of depth  $D$ ,  $D = 1, \dots, 8$ . Symbols denote mean values of 20 cells selected at random from each sublayer. Each curve corresponds to a particular choice of model parameters; plots of the experimental data from Fig. 3 are added for comparison. Threshold parameters were  $t_0 = 2.20$  and  $t_1 = 11.25$  (a) Convergence of M1- and M2-inputs: Each curve refers to the corresponding thalamic weight distribution of Fig. 7. LGN parameters were taken from Table 2 (P cells), Table 3a, b (M2 + M1 cells; Set D). (b) Plots of response properties for different receptive field parameters of the LGN-M1 and LGN-M2 cells. The parameters for the different datasets are listed in Table 3a; contrast gains and maximum firing rates were identical for both LGN-M populations and taken from Table 2. The thalamic weight distribution was taken from Fig. 7. (c) Plots of response properties for different receptive field parameters, contrast gains and maximum spike rates of the LGN-M1 and LGN-M2 cells. The parameters for the different datasets are listed in Table 3a, b. The thalamic weight distribution was taken from Fig. 7b.

## 5. Discussion

Our simulation results suggest that the rapid rate of change in field size and contrast sensitivity values through the upper half of layer 4C $\alpha$  cannot be due to purely feedforward excitation from what we have called the classical thalamic input i.e. single populations of M and P fibers that have individual axon arbors distributed through the depth of the upper and lower halves of layer 4C respectively. Interestingly, however, the simulation provides a good match for the real physiological data through the lower half of the layer and just over the border into 4C $\alpha$  suggesting that the concept of dendritic overlap across the  $\alpha/\beta$  border

allowing single neurons to sample both M- and P-input is likely to have functional relevance.

While the real physiological data could not be matched using single M- and P-LGN cell populations, when we introduced two populations of M fibers with partial terminal overlap in upper 4C $\alpha$  and with response properties constrained within the known range for LGN-M cells, a very close match to the physiological data from more than one laboratory could be obtained with simple feedforward excitation. Using staggered dendritic overlap of the spiny stellate neurons and changing weight of synaptic input from these three fiber sets (P, M1, M2), realistic response properties were achieved.

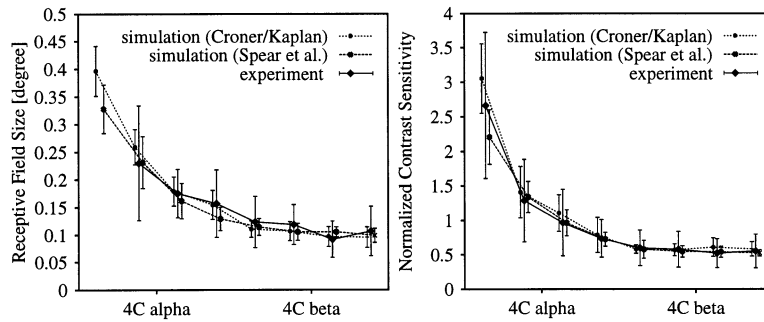


Fig. 9. Best fits for receptive field size and contrast sensitivity curves for model II (two LGN-M populations) based on the Croner & Kaplan (1995) and Spear, Moore, Kim, Xue & Tumosa (1994) data sets. The plots show mean values and standard deviations for the eight layers of model-layer 4C. Left column: Receptive field size as a function of depth. Threshold parameters were  $t_0 = 2.20$  (for Croner & Kaplan, 1995) and  $t_0 = 1.25$  (Spear, Moore, Kim, Xue & Tumosa (1994)). Right column: Normalized contrast sensitivity as a function of depth. Threshold parameters were  $t_1 = 11.25$  (for Croner & Kaplan, 1995) and  $t_1 = 8.50$  (Spear, Moore, Kim, Xue & Tumosa (1994)). The physiological parameters of P, M2 and M1 population are listed in Table 2, Table 3a, b and the thalamic weight portions are given in Table 4. For the definition of cortical threshold parameters see Section 3.5.2

We have earlier reviewed the fragmentary anatomical and physiological data that exists concerning the presence of two M fiber groups terminating in layer 4C $\alpha$ . We suggest that the results of this modeling study provide a strong impetus for further examination of the M cells in the LGN and their inputs to the striate cortex. The model shows that certain characteristics given to the population we term LGN-M1 input: their larger receptive field sizes, higher contrast sensitivity, wider axon arborization and restricted termination to the upper half of 4C $\alpha$  compared to the LGN-M2-input, may be crucial identifiers of this fiber population.

As mentioned in our review of the literature, physiological data with corrected laminar boundaries shows the fastest conducting (i.e. largest diameter) M axons to terminate in upper 4C $\alpha$  (Bullier & Henry, 1980). Sampling problems in recording from LGN units may, however, have precluded recognition of a distinct M1 population since our model suggests the M1 population need be no more frequent than 12% of LGN-M cells. It is also apparent that there can be some overlap in properties in the two M populations without significant loss of the match between model and real physiological data. This is important since recent extensive quantitative characterizations of the macaque LGN (Spear, Moore, Kim, Xue & Tumosa, 1994; Levitt, Schumer, Sherman, Spear & Movshon, 1998) have failed to reveal distinct subclasses of M neurons. We suggest that features to search for in new physiological studies aimed at identifying distinct M subpopulations might include investigation of firing rates and patterns of response in LGN-M cells; in layer 4C postsynaptic cell NMDA and non-NMDA EPSPs in relation to input conduction velocity might produce useful signatures; and in both layer 4C and M layers of the LGN an investigation of cells following 60 Hz refresh rate of the stimulus monitor or having fast oscillatory responses could be useful.

It is important to ask if factors other than direct

excitatory input from the LGN could determine the increasingly rapid change in properties with rise in depth of layer 4C. One factor that might enter into differences in receptive field size and contrast sensitivity of neurons at the top of layer 4C $\alpha$  is differences in inhibition to the spiny stellate neurons at different depths in layer 4C. A decreasing level of inhibition with movement up in the layer could give a decreasing threshold to thalamic input. This in turn could lead to a larger apparent receptive field size and higher contrast sensitivity in neurons higher in the layer. However, in our own unpublished electron microscopic studies there appears to be no significant difference in number of type 2 (GABAergic) synapses per unit area of cell soma surface through the depth of layer 4C. There may, however, be different numbers of inhibitory contacts on the dendrites or inhibition coming from different interneuron types that could lead to different thresholds.

Table 4

Optimal proportions of P-, M1- and M2-inputs to spiny stellate cells as a function of depth in layer 4C for the results shown in Fig. 9

Depth (D)	Layer 4C $\alpha$ (%)				Layer 4C $\beta$ (%)			
	8	7	6	5	4	3	2	1
LGN-P	0	0	13/10	35	65	87	100	100
LGN-M2	25/17	62/50	87/72	65	35	13	0	0
LGN-M1	75/83	38/50	0/18	0	0	0	0	0

The table shows the thalamic weight portions  $W^{\text{LGN-P}}(D)$ ,  $W^{\text{LGN-M1}}(D)$  and  $W^{\text{LGN-M2}}(D)$  at eight discrete depths of layer 4C for the Croner & Kaplan (1995) data, left numbers, and the Spear, Moore, Kim, Xue & Tumosa (1994) data, right numbers. If only one number is specified equal values were obtained for both datasets. While it was sufficient to assign thalamic M1-input to the top of layer 4C $\alpha$  ( $D = 8, 7$ ) in case of the Croner & Kaplan (1995) data, the Spear, Moore, Kim, Xue & Tumosa (1994) data suggest M1-input also to neurons deeper in the  $\alpha$  subdivision ( $D = 6$ ).

Another factor that could lead to the change in response properties in depth of layer 4C is the presence of lateral excitatory connections known to exist between the spiny stellate neurons. These connections increase in lateral spread in stepwise fashion from the lower third, to mid third, to upper third of layer 4C (Fitzpatrick, Lund & Blasdel 1985; Yoshioka, Levitt & Lund, 1994) being widest in upper 4C $\alpha$ . The lateral connections could potentially create the large receptive fields (and higher contrast sensitivities) in upper 4C $\alpha$  rather than the receptive fields being due to direct M1-input as we have proposed in our model. It might be expected that in such circumstances the earliest responses from upper 4C $\alpha$  neurons should convey a smaller receptive field than the later parts of the response; or that earlier responding neurons should have smaller receptive fields than later responding neurons (on which the earlier responders—perhaps the purely intrinsically projecting cells—terminate) at the same depth in layer 4C. However, in support of the hypothesis that direct thalamic relays may be the effective determinant of the basic properties we have modeled, we have used: (i) data of Blasdel & Fitzpatrick (1984) who recorded from a population of non-oriented cells, which are most likely to be first order cells; and (ii) data of Hawken & Parker (1984) who recorded from a group of orientation specific cells which are more likely to receive lateral recurrent input (in addition to thalamic input) refining or even inducing orientation specific responses; since both data sets show the same form of progression in contrast sensitivity with depth, our interpretation is that contrast sensitivity can be accounted for by the pattern of direct thalamic input. As well, we have demonstrated that realistic dendritic overlap and feedforward excitation is sufficient to explain neuron properties in the lower two-thirds of layer 4C—despite there being an abrupt change in length of lateral connections halfway through layer 4C $\beta$ . In addition, despite their small number relative to intrinsic lateral connections, the thalamic inputs drive spiny stellate neurons (in cat V1 layer 4) with large and reliable EPSPs whereas the intracortical synaptic connections are individually less reliable than thalamic inputs as a driving force (Stratford, Tarczyhorno, Martin & Jack, 1996). These are parameters that will be simulated in future versions of our model, which will include recurrent intracortical connections, and as well be examined in new anatomical and physiological experiments.

If our model is correct in predicting two M populations, it is the M1-input that is almost entirely restricted to neurons projecting to layer 4B and perhaps predominating in driving the generation of direction selectivity that is seen in upper 4C $\alpha$  and in layer 4B. The large axons presumed to be M1 axons, provide extensive collateral input to layer 6 which also contains direction

selective neurons (Blasdel & Lund, 1983; Hawken, Parker & Lund, 1988; Freund, Martin, Soltesz, Somogyi & Whitteridge, 1989). The M2 population, while contributing to neurons in upper 4C $\alpha$  has a primary role in combining with P-input to neurons of mid layer 4C; these neurons project to the superficial layers, particularly to interblob territories of layer 3B. Pure P-input is seen predominantly in neurons of the lower half of 4C $\beta$  and their relays pass on to engage layer 4A, itself the recipient of direct LGN P-input.

## 6. Summary

Purely feedforward excitation has proved sufficient to produce a good match to the physiologically observed response properties of layer 4C neurons. The model predicts that: (i) there are two M pathways entering layer 4C $\alpha$  with different emphasis of the range of properties currently assigned to M cells in the LGN; (ii) that dendritic overlap in depth of layer 4C allows single cells to receive both M- and P-inputs; and (iii) that inhibition is not an essential determinant of the size of the minimum response field and contrast sensitivity of layer 4C neurons.

## Acknowledgements

Supported by MRC-G9203679N, MRC-G9408137, NIH-EY10021 and HFSP grant RG-98/94, Wellcome Trust grant no. 050080/z/97/z, a scholarship from the DFG-Graduiertenkolleg 231 and DFG grant Ob 102/2-1.

## References

- Anderson, J. C., Douglas, R. J., Martin, K. A. C., & Nelson, J. C. (1994). Map of the synapses formed with the dendrites of spiny stellate neurons of cat visual cortex. *Journal of Comparative Neurology*, *341*, 25–38.
- Bauer, U., Scholz, M., Levitt, J. B., Obermayer, K., & Lund, J. S. (1997). A neural network model of geniculocortical information transfer in primate visual system. In N. Elsner & H.-U. Schnitzler. Proceedings of the 25th Goettingen neurobiology conference. Stuttgart: Georg Thieme.
- Blasdel, G. G., & Fitzpatrick, D. (1984). Physiological organization of layer 4 in macaque striate cortex. *Journal of Neuroscience*, *4*(3), 880–895.
- Blasdel, G. G., & Lund, J. S. (1983). Termination of afferent axons in macaque striate cortex. *Journal of Neuroscience*, *3*, 1389–1413.
- Bullier, J., & Henry, G. H. (1980). Ordinal position and afferent input of neurons in monkey striate cortex. *Journal of Comparative Neurology*, *193*, 913–935.
- Carey, R., Bear, M., & Diamond, I. (1980). The laminar organization of the reciprocal projections between the claustrum and the striate cortex in the tree shrew, *Tupaia glis*. *Brain Research*, *184*, 193–198.

- Chow, K., Blum, J. S., & Blum, R. A. (1950). Cell ratios in the thalamocortical visual system of *Macaca mulatta*. *Journal of Comparative Neurology*, 92, 227–239.
- Connolly, M., & van Essen, D. (1984). The representation of the visual field in parvocellular and magnocellular layers of the lateral geniculate nucleus in the macaque monkey. *Journal of Comparative Neurology*, 226, 544–564.
- Croner, L. J., & Kaplan, E. (1995). Receptive fields of P and M ganglion cells across the primate retina. *Vision Research*, 35(1), 7–24.
- Das, A. (1996). Orientation in visual cortex: A simple mechanism emerges. *Neuron*, 16, 477–480.
- Derrington, A. M., & Lennie, P. (1984). Spatial and temporal contrast sensitivities of neurones in lateral geniculate nucleus of macaque. *Journal of Physiology (London)*, 357, 219–240.
- Enroth-Cugell, C., & Robson, J. G. (1966). The contrast sensitivity of retinal ganglion cells of the cat. *Journal of Physiology*, 187, 517–552.
- Fitzpatrick, D., Lund, J. S., & Blasdel, G. G. (1985). Intrinsic connections of macaque striate cortex: Afferent and efferent connections of layer 4C. *Journal of Neuroscience*, 5, 3329–3349.
- Freund, T. F., Martin, K. A. C., Soltesz, I., Somogyi, P., & Whitteridge, D. (1989). Arborisation pattern and postsynaptic targets of physiologically identified thalamocortical afferents in striate cortex of the macaque monkey. *Journal of Comparative Neurology*, 289, 315–336.
- Hawken, M. J., & Parker, A. J. (1984). Contrast sensitivity and orientation selectivity in lamina IV of the striate cortex of old world monkeys. *Experimental Brain Research*, 54, 367–372.
- Hawken, M. J., Parker, A. J., & Lund, J. S. (1988). Laminar organisation and contrast sensitivity of direction selective cells in the striate cortex of the old world monkey. *Journal of Neuroscience*, 8, 3541–3548.
- Hicks, T. P., Lee, B. B., & Vidyasagar, T. R. (1983). The responses of cells in macaque lateral geniculate nucleus to sinusoidal gratings. *Journal of Physiology (London)*, 337, 183–200.
- Hubel, D. H., & Wiesel, T. N. (1972). Laminar and columnar distribution of geniculocortical fibers in macaque monkey. *Journal of Comparative Neurology*, 146, 421–450.
- Kaplan, E., & Shapley, R. M. (1982). X and Y cells in the lateral geniculate nucleus of macaque monkeys. *Journal of Physiology (London)*, 330, 125–143.
- LeVay, S., & Sherk, H. A. (1981). The visual claustrum of the cat: I. Structure and connections. *Journal of Neuroscience*, 1, 956–980.
- Leventhal, A. G., Rodieck, R. W., & Dreher, B. (1981). Retinal ganglion cell classes in old world monkey: morphology and central projections. *Science*, 213, 1139–1142.
- Levitt, J. B., Schumer, R. A., Sherman, S. M., Spear, P. D., & Movshon, J. A. Receptive field properties of neurons in the lateral geniculate nucleus of normally-reared and visually-deprived macaque monkeys. (In preparation).
- Linsenmeier, R. A., Frishman, L. J., Jakiela, H. G., & Enroth-Cugell, C. (1982). Receptive field properties of x and y cells in the cat retina derived from contrast sensitivity measurements. *Vision Research*, 22, 1173–1183.
- Livingstone, M. S., & Hubel, D. H. (1987). Psychophysical evidence for separate channels for the perception of form, colour, movement and depth. *The Journal of Neuroscience*, 7(11), 3417–3468.
- Livingstone, M. S., & Hubel, D. H. (1988). Do the relative mapping densities of magno- and parvocellular systems vary with eccentricity? *Journal of Neuroscience*, 8(11), 4334–4339.
- Lund, J., Wu, Q., Hadingham, P. T., & Levitt, J. B. (1995). Cells and circuits contributing to functional properties in area V1 of macaque monkey cerebral cortex: Bases for neuroanatomically realistic models. *Journal of Anatomy (London)*, 187, 563–581.
- Lund, J. S. (1973). Organisation of neurons in the visual cortex of the monkey (*Macaca mullata*). *Journal of Comparative Neurology*, 147, 455–496.
- Lund, J. S. (1980). Intrinsic organization of the primate visual cortex, area 17, as seen in Golgi preparations. The organization of the cerebral cortex: proceedings of a neuroscience research program colloquium. MIT Press: Cambridge, MA, pp. 105–124.
- Lund, J. S. (1990). Excitatory and inhibitory circuitry and laminar mapping strategies in primary visual cortex of the monkey. In G. M. Edelman, W. E. Gall, & W. M. Cowan, *Signal and Sense: local and global order in perceptual maps*. New York, NY: John Wiley and Sons, 51–66.
- Lund, J. S., & Holbach, S. (1991). Postnatal development of thalamic recipient neurons in monkey striate cortex: I. a comparison of spine acquisition and dendritic growth of layer 4C $\alpha$  and 4C $\beta$  spiny stellate neurons. *Journal of Comparative Neurology*, 309, 115–128.
- Lund, J. S., Levitt, J. B., & Wu, Q. (1994). Topography of excitatory and inhibitory connectional anatomy in monkey visual cortex. In T. B. Lawton, *Computational vision based on neurobiology*. Asilomar, CA: International Society of Optical Engineering (SPIE), 174–184.
- Maunsell, J. H. R., & Gibson, J. R. (1992). Visual response latencies in striate cortex of the macaque monkey. *Journal of Neurophysiology*, 68(4), 1332–1344.
- Naka, K.-I., & Rushton, W. A. H. (1966). S-potentials from luminosity units in the retina of fish (*Cyprinidae*). *Journal of Physiology (London)*, 185, 587–599.
- Nowak, L. G., Munk, M. H. J., Girard, P., & Bullier, J. (1995). Visual latencies in area V1 and V2 of the macaque monkey. *Visual Neuroscience*, 12, 371–384.
- O’Kusky, J., & Colonnier, M. (1982). Postnatal changes in the number of neurons and synapses in the visual cortex (area 17) of the macaque monkey: A stereological analysis in normal and monocularly deprived animals. *Journal of Comparative Neurology*, 210, 291–306.
- Peters, A., Payne, B. R., & Budd, J. (1994). A numerical analysis of the geniculocortical input to striate cortex in the monkey. *Cerebral Cortex*, 4, 215–229.
- Rodieck, R. W. (1965). Quantitative analysis of cat retinal ganglion cell response to visual stimuli. *Vision Research*, 5, 583–601.
- Sclar, G., Maunsell, J. H. R., & Lennie, P. (1990). Coding of image contrast in central visual pathways of the macaque monkey. *Vision Research*, 30(1), 1–10.
- Shapley, R. (1990). Visual sensitivity and parallel retinocortical channels. *Annual Review of Psychology*, 41, 635–658.
- Spear, P. D., Moore, R. J., Kim, C. B. Y., Xue, J.-T., & Tumosa, N. (1994). Effects of aging on the primate visual system: Spatial and temporal processing by lateral geniculate neurons in young adult and old rhesus monkeys. *Journal of Neurophysiology*, 72(1), 402–420.
- Stratford, K., Tarczyhornoch, K., Martin, K., & Jack, J. (1996). Excitatory synaptic inputs to spiny stellate cells in cat visual cortex. *Nature*, 382, 258–261.
- Van Essen, D. C., Newsome, W. T., & Maunsell, J. H. R. (1984). The visual field representation in striate cortex of macaque monkey: asymmetries, anisotropies, and individual variability. *Vision Research*, 24(5), 429–448.
- Wu, Q., Lund, J. S., & Levitt, J. B. (1994). Anatomically based neural network model of the circuitry within layer 4C of primary visual cortex (V1) in macaque. *Investigative Ophthalmology and Visual Science*, 35, 1828.
- Yoshioka, T., Levitt, J. B., & Lund, J. S. (1994). Independence and merger of thalamocortical channels within macaque monkey primary visual cortex: anatomy of interlaminar projections. *Visual Neuroscience*, 11, 467–489.